PAPER

Check for updates

Hybrid polyurethane–MOF platform for turn-on fluorescent sensing of Cu²⁺ ion

Susan Sarvarian,[a] Moslem Mansour Lakouraj, [ID] *[a] Rafieh-Sadat Norouzian[a] and Mohammad Javad Chaichi[b]

The pervasive contamination of water resources by heavy metal ions poses serious threats to environmental safety and human health, creating an urgent demand for simple, sensitive, and selective sensing platforms. Herein, a robust polyurethane foam (PUF)-supported UiO-66-NH₂–calcein composite is developed as a solid-state fluorescent sensor for the selective detection of Cu²⁺ ions in aqueous media. The immobilization of calcein within the porous UiO-66-NH₂ framework and its subsequent integration into a PUF matrix provides a stable, highly accessible, and reusable fluorescence platform. Structural and spectroscopic characterization confirms the successful formation and homogeneous distribution of the composite components. Fluorescence screening against a series of metal ions demonstrates that, although several ions can interact with the sensor, a markedly enhanced and selective fluorescence response toward Cu²⁺ is achieved under mildly acidic conditions (pH 5). The sensor exhibits a linear fluorescence response toward Cu²⁺ over the micromolar concentration range with a low detection limit of 0.011 μM. The composite also exhibits mechanical integrity and operational reusability, with no significant signal loss. The foam-based architecture enables rapid mass transfer, improved light penetration, and convenient handling, making the platform well-suited for portable and on-site water analysis. This work presents an effective strategy for constructing MOF–polymer fluorescent composites for selective Cu²⁺ sensing and practical environmental monitoring. The PUF/UIO-66-NH–calcein nanocomposite exhibits remarkable fluorescence sensitivity toward multiple metal ions at pH 7, achieving ultra-low limits of detection of 0.0013 μM for As³⁺, 0.0049 μM for Cd²⁺, 0.009 μM for Zn²⁺, 0.0049 μM for Cu²⁺, and 0.0081 μM for Ca²⁺, while maintaining stable performance under aqueous conditions.

1. Introduction

The contamination of aquatic environments with heavy metal ions, originating mainly from industrial discharge and anthropogenic activities, represents a critical threat to ecological systems and human health. Toxic metals such as cadmium (Cd²⁺), lead (Pb²⁺), mercury (Hg²⁺), arsenic (As³⁺), and copper (Cu²⁺) ions are non-biodegradable and can accumulate in living organisms through the food chain. Their long-term exposure is associated with severe biological effects, including oxidative stress, disruption of protein and DNA functions, tumors and the development of chronic diseases such as neurological disorders, renal dysfunction, and cancer.[1,2]

Among heavy metals, copper occupies a unique position as both an essential trace element and a potential toxicant. Copper ions play indispensable roles in numerous physiological processes, including enzymatic catalysis, cellular respiration, and redox regulation. However, an imbalance in Cu²⁺ levels, either deficiency or excess, can result in a wide range of pathological conditions.[3] Elevated copper concentrations have been linked to gastrointestinal distress, liver and kidney damage, neurodegenerative diseases, and oxidative injury caused by the generation of reactive oxygen species (ROS). According to the U.S. Environmental Protection Agency (EPA), the maximum allowable concentration of Cu²⁺ in drinking water is 1.3 ppm.[4] Therefore, the development of sensitive and selective methods for monitoring Cu²⁺ ions is of great importance for environmental and biomedical applications.

Conventional analytical techniques such as atomic absorption spectroscopy (AAS), inductively coupled plasma mass spectrometry (ICP-MS), and electrochemical methods provide high accuracy and reliability. Nevertheless, their dependence on sophisticated instrumentation, skilled personnel, and extensive sample preparation limits their applicability for rapid and on-site analysis. In contrast, fluorescence-based sensing strategies have emerged as powerful alternatives owing to their high

[a]Polymer chemistry research laboratory, Department of Organic Chemistry, Faculty of Chemistry, University of Mazandaran, Babolsar 47416-95447, Iran. E-mail: lakouraj@umz.ac.ir; lilisarvarian@gmail.com; r.norouzian@umz.ir

[b]Department of Analytical Chemistry, Faculty of Chemistry, University of Mazandaran, Babolsar, Iran. E-mail: jchaichi@yahoo.com

sensitivity, rapid response, operational simplicity, and potential for miniaturization and portability.

A typical fluorescent sensor consists of a recognition unit, a fluorophore, and a connecting spacer. Interaction between the target ion and the receptor induces changes in the optical properties of the fluorophore, leading to either fluorescence enhancement or quenching. These signal transduction processes are commonly governed by mechanisms such as photoinduced electron transfer (PET), intramolecular charge transfer (ICT), fluorescence resonance energy transfer (FRET), or chelation-enhanced fluorescence (CHEF).[5–8] In recent years, extensive efforts have been devoted to the design of fluorescent and fluorescent/colorimetric probes for Cu^{2+} detection due to their low cost, simplicity, and high sensitivity.[9,10] Despite significant progress, many reported systems still suffer from limitations, including complex synthesis routes, insufficient sensitivity, narrow working pH ranges, low quantum yields, and poor selectivity in the presence of competing metal ions.[11] These challenges highlight the need for developing new sensing platforms that combine simplicity, robustness, and high selectivity toward Cu^{2+}.

Among the fluorescent materials, those whose fluorescence increases significantly in the presence of the target are especially useful due to their low background noise and clear signal. Recently, metal–organic frameworks (MOFs) have attracted considerable attention as sensor platforms. These materials, made by the coordination of metal ions with organic linkers, are porous, customizable, and have large surface areas.[12–16] Zirconium-based MOFs, *i.e.*, UIO-66-NH₂, are particularly attractive because they're chemically stable and easy to modify, making them excellent hosts to support fluorescent molecules. Different approaches, like *in situ* doping or guest encapsulation, enable the introduction of specific sensing sites into MOFs.[17–21] Calcein, a commercial fluorescent dye with high metal-binding affinity, is especially effective in water-based sensing systems.[22] Although calcein exhibits high fluorescence intensity, its solubility limits the reusability in aqueous sensing systems. To overcome this drawback, we planned to immobilize it on UIO-66-NH₂, which provides a stable framework to prevent dye leaching. In addition, an additional support with high stability and porosity is designed for practical usability and easy recovery of the functionalized MOF. Nanoparticles and functional compounds are often encapsulated or immobilized within polymer matrices or porous supports such as zeolites to enhance their stability, prevent aggregation, and enable their efficient utilization in various functional applications.[23,24] Polyurethane foam (PUF), with its interconnected microporous structure and mechanical robustness,[25,26] was therefore selected as the host matrix for stabilizing the MOF–calcein. This not only immobilizes the MOF–calcein composite but also allows heavy metal ions to diffuse into the pores and interact efficiently with the sensing sites, ensuring reliable fluorescence detection in real water environments.

In this study, a new efficient fluorescent sensor was developed by embedding calcein-doped UIO-66-NH₂ into a flexible PUF matrix (Scheme 1). The uniform distribution of functionalized MOF in flexible PU matrix stabilizes the MOF's

constituents and makes the solute fundamentally accessible to sensing sites and easy to interact with. For this purpose, UIO-66-NH₂ is prepared by the solvothermal method and then functionalized with calcein *via* direct amidation reaction. In the second step, the functionalized MOF was embedded in the PU network to enhance stability and improve the sensor's properties and usability. The final nanocomposite is expected to exhibit a strong and selective fluorescence response to various heavy metals, with a clear linear relationship to their concentrations. This approach offers a practical, scalable, and cost-effective solution for real-time water quality monitoring.

2. Experimental section

2.1. Materials

Zirconium chloride (ZrCl₄), 2-aminoterephthalic acid, dibutyltin dilaurate, calcein, *N,N'*-dicyclohexylcarbodiimide (DCC), and 4-dimethylaminopyridine (DMAP) were purchased from Merck. Other chemicals, including *N,N*-dimethylformamide (DMF), acetic acid, glycerol, silicone surfactant, 1,4-diazabicyclo[2.2.2]octane (DABCO), 2,4-toluene diisocyanate (TDI), and polyether polyol, were obtained from commercial suppliers in China. All reagents were of analytical grade and used without further purification.

2.2. Instrumentation

All analytical measurements were performed using standard high-precision instrumentation.

FT-IR spectra were obtained on a Bruker Tensor II spectrometer using KBr pellets to identify functional groups and to investigate interfacial interactions between the MOF and PU matrix. Thermal stability and decomposition profiles were evaluated using thermogravimetric analysis (TGA) on a STA6000 analyzer at a heating rate of 10 °C min⁻¹. Powder X-ray diffraction (XRD) patterns were recorded on a Philips XP diffractometer over $2\theta = 5$–80. Scanning electron microscopy (SEM) was used to observe surface morphology and MOF dispersion within the PU matrix using a Tescan Mira 3 FE-SEM. Textural properties, including BET surface area and pore size distribution, were determined by N₂ adsorption–desorption measurements using the BET Belsorp system. Fluorescence spectra were collected on a JASCO FP-8300 spectrofluorometer equipped with a xenon lamp for both solution-phase and solid-state analyses.

2.3. Synthesis of UiO-66-NH₂

UIO-66-NH₂ was synthesized using a modified solvothermal method by dissolving 1 mmol of ZrCl₄ and 1 mmol of 2-aminoterephthalic acid separately in 50 mL of DMF. The solutions were mixed and sonicated for 20 minutes, and then heated at 120 °C for 24 hours. The resulting solid was collected by vacuum filtration, washed with DMF and acetone, and finally dried under vacuum at 80 °C for 6 hours[27] (Scheme 1).
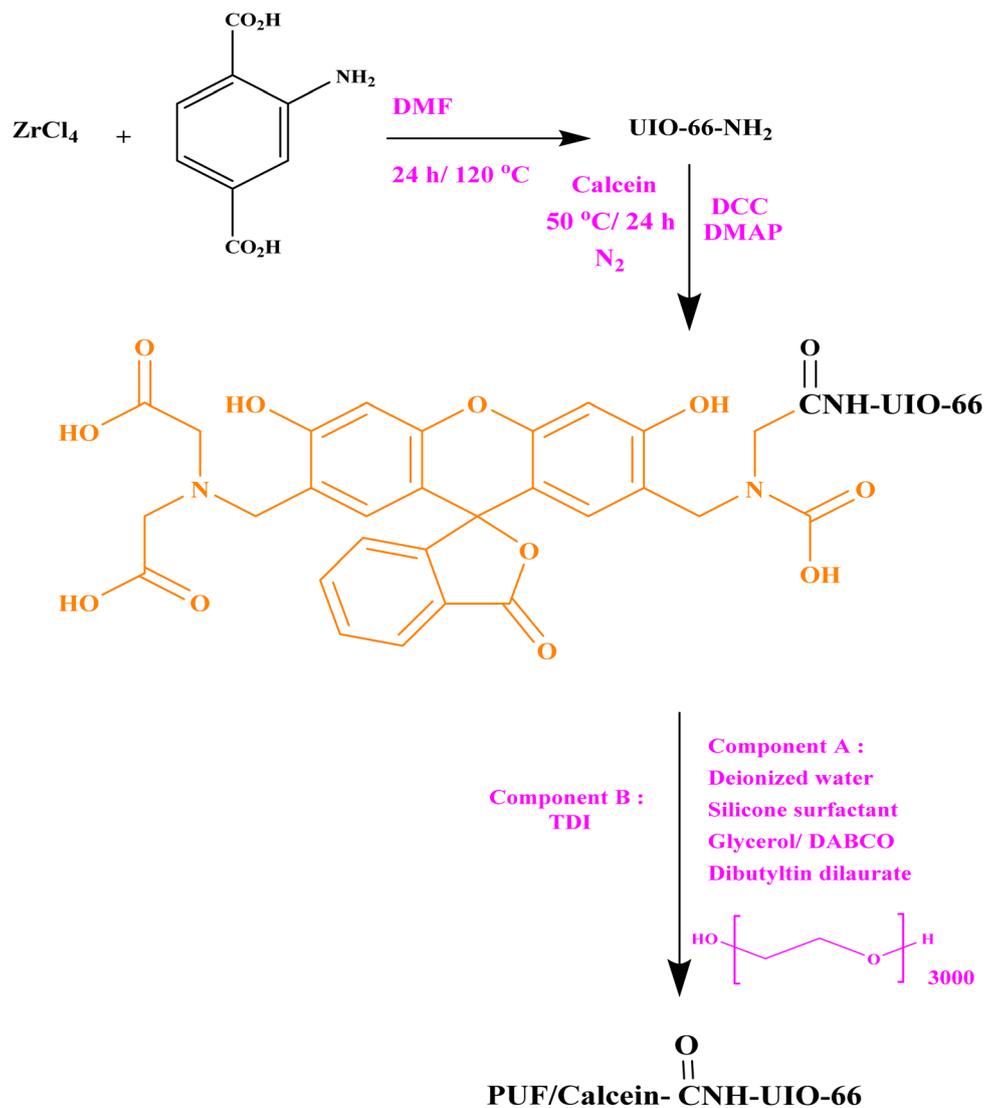
Scheme 1 Schematic illustration of the synthetic pathway for preparation of UIO-66-NH$_2$, covalent attachment of calcein to the UIO-66-NH$_2$ framework, and PUF/UIO-66-NH-calcein nanocomposite.

2.4. MOF functionalization with calcein

To immobilize calcein onto the MOF structure (Scheme 1), 1 mmol of UIO-66-NH$_2$ and 2 mmol of calcein were dispersed in 20 mL of dry DMF under a nitrogen atmosphere, and stirred at 60 °C for 30 minutes. Then, 2 mmol of DCC (in 5 mL DMF) was added dropwise. After 10 minutes, 2 mmol of DMAP dissolved in 5 mL of DMF was added. The reaction mixture was kept under nitrogen and stirred at 60 °C for 24 hours. The product was separated by centrifugation, thoroughly washed with deionized water and ethanol, and dried under vacuum at 60 °C.

2.5. Fabrication of PUF/UIO-66-NH-calcein nanocomposite

To prepare the nanocomposite foam, polyurethane components A and B were formulated following standard procedures.[28] A known amount of UIO-66-NH-calcein powder was added to component A, which included 10 mL of polyether polyol, 1 mL of deionized water, 1 mL of glycerol, 1 wt% silicone surfactant

(relative to polyol), and small catalytic amounts of DABCO and dibutyltin dilaurate (0.001 wt% each) and dispersed by ultrasonication for 2 minutes to ensure uniform distribution. Component B (TDA) was then added, and the mixture was stirred mechanically at 800 rpm for 1 minute. The resulting mixture was poured into a silicone mold and cured at room temperature. After curing, the foam was cut into uniform samples (1 cm × 1 cm × 0.5 cm) for further testing (Fig. 1).

2.6. Fluorescence sensing studies

The fluorescence sensing performance of the PUF/UiO-66-NH–calcein nanocomposite was evaluated using fluorescence spectroscopy. A fixed amount of the nanocomposite was immersed in aqueous solutions containing various metal ions (e.g., Cu^{2+}, Zn^{2+}), and the emission spectra were recorded under identical excitation conditions. The nanocomposite exhibited a characteristic fluorescence response arising from the coordination of
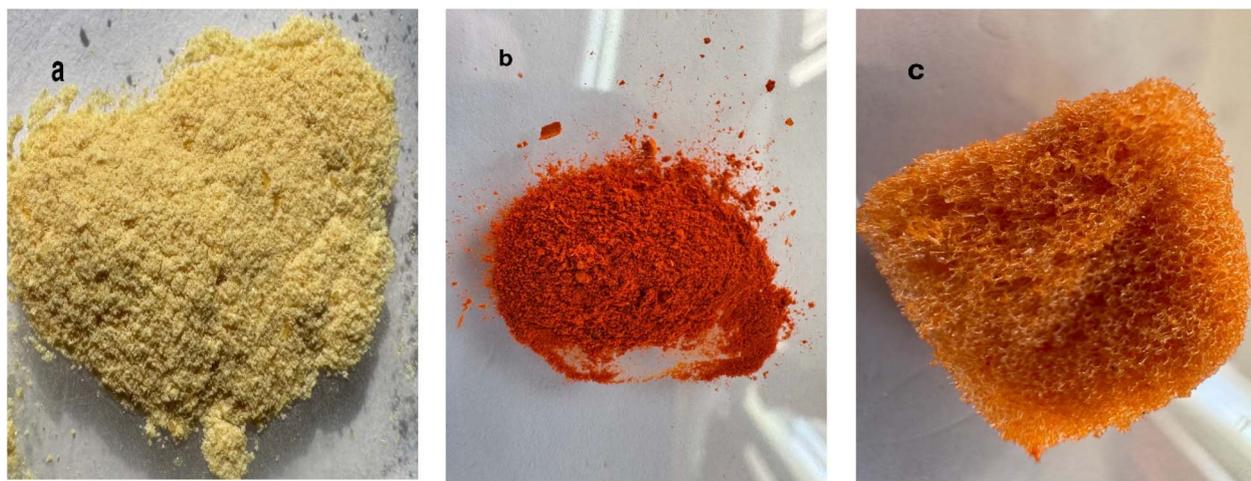
Fig. 1 Photographic images of the synthesized (a) UIO-66-NH$_2$, (b) UIO-66-NH–calcein, and (c) PUF/UIO-66-NH–calcein nanocomposite.

metal cations with the reactive calcein sites anchored within the MOF structure. Upon exposure to different metal ions, distinct changes in fluorescence intensity—either enhancement or quenching—were observed, depending on the specific metal–ligand interaction mechanism. These fluorescence variations are attributed to the coordination of metal ions with the carboxylate and phenolic groups of calcein, potentially involving electron transfer or energy transfer processes. Comparative emission analyses further confirmed the superior selectivity of the PUF/UiO-66-NH–calcein nanocomposite toward Cu^{2+} ions.

3. Results and discussion

The PUF/UiO-66-NH–calcein nanocomposite was successfully synthesized through a stepwise fabrication process, as illustrated in Scheme 1. The resulting hybrid material was subsequently subjected to comprehensive physicochemical characterization, as discussed in the following sections.

3.1. FTIR characterization

The FTIR spectrum of pristine UiO-66-NH$_2$ (Fig. 2a), exhibits a broad absorption band centered around 3400 cm^{-1}, corresponding to the N–H stretching vibrations of amino groups and hydrogen-bonded –NH$_2$ functionalities. The characteristic asymmetric and symmetric stretching vibrations of carboxylate groups appear at 1650–1660 cm^{-1}, while the band observed at 750–800 cm^{-1} is assigned to Zr–O–Zr vibrations, which are typical of the UiO-66 framework.[27] After calcein functionalization (Fig. 2b), a noticeable decrease in the intensity of the –NH$_2$ stretching band is observed, indicating covalent interactions between the amino groups of the MOF and the carboxylic acid groups of calcein. The appearance of a new peak near 1730 cm^{-1} is attributed to the stretching vibration of free carbonyl (C=O) groups of calcein. Additionally, bands in the range of 1250–1150 cm^{-1} correspond to C–O–C stretching vibrations, further confirming the successful incorporation of the dye into the
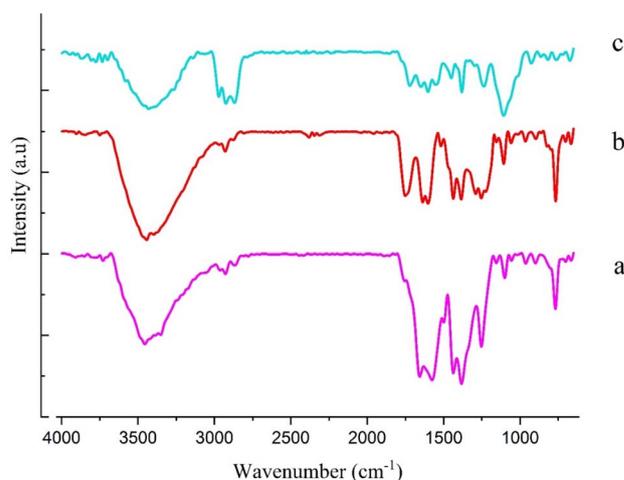

Fig. 2 The FTIR spectra of (a) UIO-66-NH$_2$, (b) UIO-66-NH–calcein, and (c) PUF/UIO-66-NH–calcein.

MOF structure. In the FTIR spectrum of the PUF/UiO-66-NH–calcein nanocomposite (Fig. 2c), new absorption bands at 2920 and 2850 cm^{-1} are assigned to the C–H stretching vibrations of the polyurethane backbone, while the strong band near 1700 cm^{-1} corresponds to the urethane C=O stretching vibration. The broadening of the N–H stretching band around 3300 cm^{-1} suggests the presence of hydrogen-bonding interactions between the PU chains and the MOF–calcein hybrid. The coexistence of characteristic vibrational features from PU, MOF, and calcein clearly confirms the successful fabrication of a stable hybrid nanocomposite through both chemical and physical interactions (Fig. 2).

3.2. 2. SEM analysis

The morphology of UiO-66-NH–calcein and the PUF/UiO-66-NH–calcein nanocomposite was investigated using scanning electron microscopy (SEM). As shown in Fig. 3, SEM images of calcein-functionalized UiO-66-NH$_2$ reveal no significant change
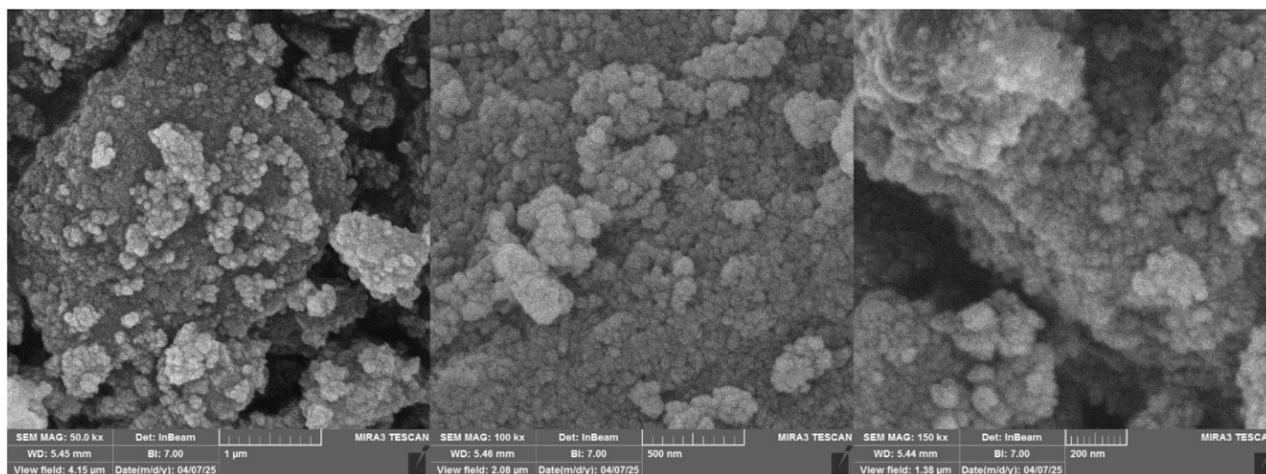
Fig. 3 SEM images of calcein-functionalized UIO-66-NH$_2$ particles.

in particle morphology compared to the pristine MOF.[29] The particles remain predominantly spherical and tend to form agglomerated clusters. Higher-magnification images (100–200 nm) reveal increased surface roughness after calcein functionalization, which can be attributed to the presence of dye molecules on the MOF surface. These roughened surfaces likely facilitate additional interactions between calcein and the amino groups of the MOF through covalent bonding and hydrogen bonding.

SEM images of the PUF/UiO-66-NH–calcein nanocomposite (Fig. 4) demonstrate that the functionalized MOF particles are uniformly distributed throughout the polyurethane foam matrix. The particles preserve their spherical morphology and remain structurally intact during the embedding process. Although occasional local agglomeration is observed, the majority of the modified MOF particles are well dispersed along the foam pores and channels. This homogeneous distribution and strong interfacial adhesion contribute to enhanced mechanical stability and reusability of the sensing platform. At higher magnification, the

porous architecture of the foam is clearly visible, providing interconnected channels that promote efficient mass transfer and facilitate interaction between analyte ions and the active sensing sites due to the high accessible surface area.

3.3. XRD analysis

The X-ray diffraction (XRD) pattern of pristine UiO-66-NH$_2$ (Fig. 5) exhibits distinct diffraction peaks at $2\theta \approx 7.3°$, $8.4°$, and $12.0°$, corresponding to the (111), (200), and (220) crystallographic planes of the Zr-based MOF lattice, confirming the successful formation of the UiO-66-NH$_2$ framework. The XRD pattern of calcein-functionalized UiO-66-NH$_2$ retains the main characteristic diffraction peaks of the parent MOF, particularly in the 2θ ranges of 7–$8°$ and 12–$13°$, indicating that the crystalline framework remains largely preserved after dye incorporation.[27] Following incorporation into the polyurethane foam, the XRD pattern of the PUF/UiO-66-NH–calcein nanocomposite still displays the characteristic reflections of the MOF structure, although with reduced intensity. This decrease in crystallinity is
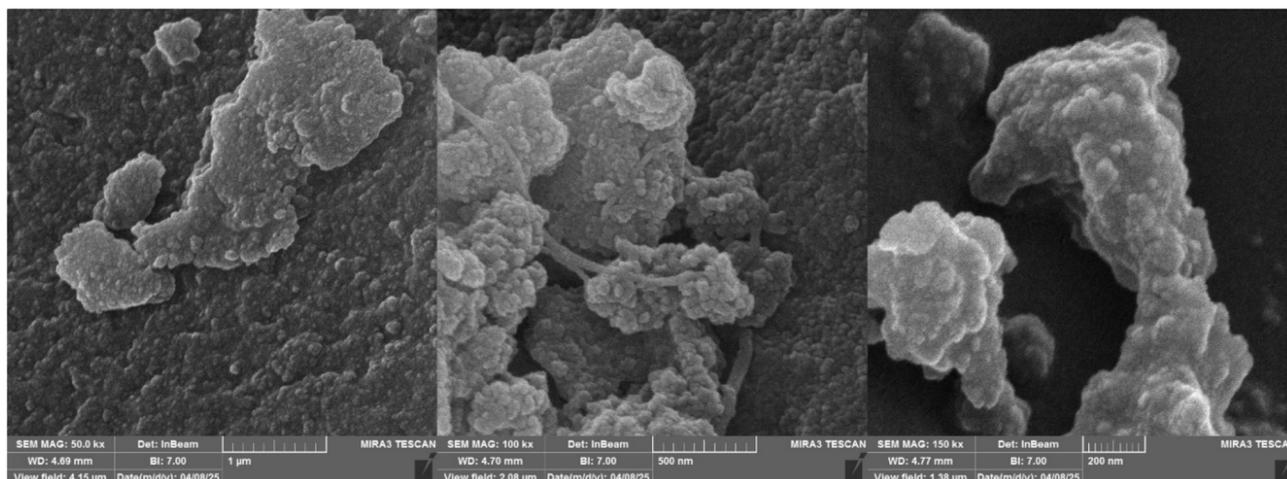

Fig. 4 SEM micrographs of the PUF/UiO-66-NH–calcein nanocomposite at different magnifications.
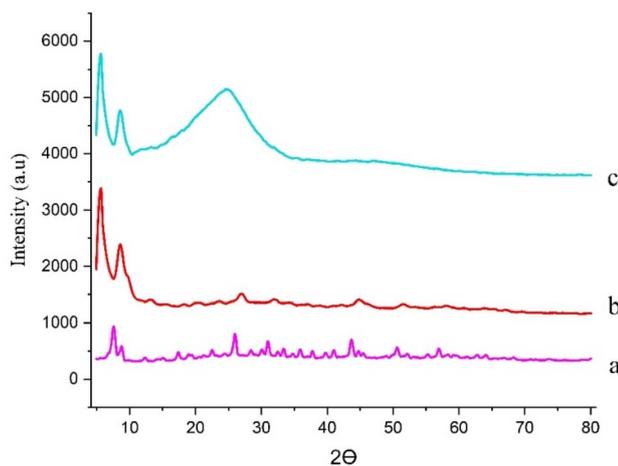
Fig. 5 XRD patterns of (a) UIO-66-NH$_2$, (b) UIO-66-NH- calcein, and (c) PUF/UIO-66-NH–calcein composite.

attributed to structural disorder induced by the embedding of the modified MOF particles within the soft and amorphous PU matrix. The partial amorphization may introduce structural defects and interfacial regions that facilitate light absorption and ion trapping, thereby contributing to enhanced sensing performance (Fig. 5).

3.4. Thermal stability

Thermogravimetric analysis (TGA) was carried out to evaluate the thermal stability of pristine UiO-66-NH$_2$ (a), UIO-66-NH–calcein, (b) and PUF/UIO-66-NH–calcein nanocomposite (c), as presented in Fig. S1. The pristine UiO-66-NH$_2$ sample (curve a) shows an initial, gradual weight loss beginning at approximately 100 °C, which can be attributed to the removal of physically adsorbed water and residual solvents trapped within the porous framework. The subsequent mass loss proceeds slowly over the full temperature range, and the material retains nearly 50% of its original weight at 600 °C, reflecting the intrinsic thermal stability of the zirconium-based MOF. For the UIO-66-NH–calcein (curve b), a minor weight loss is also observed below 150 °C, associated with moisture and weakly bound species. Notably, the main thermal degradation of the MOF–calcein begins at around 300 °C, indicating that the covalent attachment of calcein does not compromise the framework integrity. Compared with pristine UiO-66-NH$_2$, the functionalized MOF exhibits a more gradual mass–loss profile and retains approximately 60% of its weight at 600 °C, suggesting slightly enhanced thermal resistance due to additional organic–inorganic interactions. Surprisingly, the PUF/UIO-66-NH–calcein nanocomposite (curve C) remains thermally stable up to about 250 °C, after which a sharp and pronounced weight loss occurs. This major degradation step, spanning roughly 250–400 °C, is attributed to the decomposition of the polyurethane matrix.[30] As a result, the composite shows a significantly lower residual mass of around 10% at 600 °C, which corresponds to inorganic zirconium oxide and minor carbonaceous residues remaining after polymer degradation. Overall,

these results confirm that calcein functionalization preserves the thermal stability of UiO-66-NH$_2$, with the primary decomposition occurring above 300 °C, and incorporation into the PU foam alters the degradation pathway due to the dominant contribution of the polymer phase. The TGA profiles therefore support the successful formation of a structurally stable MOF–dye system embedded within a processable polymer matrix.

3.5. BET surface area and porosity analysis

The textural properties of UiO-66-NH–calcein and the PUF/UiO-66-NH–calcein nanocomposite were evaluated using nitrogen adsorption–desorption isotherms at 77 K. The pristine UiO-66-NH–calcein sample exhibits a relatively high BET surface area of 491.44 m^2 g^{-1}, indicating that the MOF framework remains largely intact after calcein functionalization. The high BET C constant (≈ 3522) suggests strong adsorbate–adsorbent interactions, likely due to the presence of free polar amino and carboxyl functional groups introduced by UiO-66-NH–calcein. The average pore diameter of 2.63 nm is consistent with a predominantly micro–mesoporous structure and a Type I adsorption isotherm. Upon incorporation of the MOF–calcein nanoparticles into the polyurethane matrix, the apparent BET surface area decreases markedly to 1.95 m^2 g^{-1}, while the average pore diameter increases to 12.78 nm. This reduction in measured surface area is attributed to partial encapsulation of MOF particles within the dense PU network, which limits nitrogen access to internal pores under cryogenic conditions. In aqueous environments, however, the porous and flexible PU matrix with long polyethylene glycol segments allows efficient diffusion of ions and small molecules, ensuring full accessibility of active sensing sites during fluorescence measurements. The low C constant (2.23) further reflects weaker interactions between nitrogen and the composite surface, consistent with the hydrophobic nature of the polymer matrix. Despite the reduced BET surface area, the PUF/UiO-66-NH–calcein hybrid nanocomposite exhibits excellent sensing performance due to several key factors: (i) enlarged interfacial pores (≈ 12–13 nm) that facilitate molecular transport and light penetration, (ii) effective immobilization of the MOF–Calcein hybrid that prevents dye leaching, and (iii) enhanced mechanical durability and reusability provided by the elastic PU framework. These combined features render the PU-based composite a robust, portable, and efficient platform for fluorescence-based metal ion detection in aqueous media (Fig. S2 and S3).

3.6. Analytical performance of PU/UIO-66-NH–calcein fluorescent sensor

The PUF/UIO-66-NH–Calcein fluorescent sensor was evaluated for its response to six metal ions: As^{3+}, Cd^{2+}, Zn^{2+}, Cu^{2+}, Ca^{2+}, and Ag$^+$. The fluorescence emission spectra of PUF/UIO-66-NH-calcein in the presence of these cations are illustrated in Fig. 9. Fluorescence measurements were performed to quantify the sensing performance of the PU/UIO-66-NH–calcein composite toward metal ions. A small cubic piece of the PU/UIO-66-NH-calcein composite foam (approximately 5 × 5 × 5 mm) was gently placed at the bottom of a standard 1 cm quartz cuvette. No

organic solvents were used in any fluorescence measurements; all experiments were conducted in deionized water. Aqueous stock solutions of Cd^{2+}, Ca^{2+}, Zn^{2+}, As^{3+}, Cu^{2+}, and Ag^+ were prepared and diluted to working concentrations of 1–5 μM. For each measurement, 2.5 mL of the desired metal ion solution (1–5 μM) was transferred into the cuvette containing the foam sensor. The system was equilibrated for 3 min to allow diffusion of ions into the porous structure. The excitation wavelength was set at λ_{max} 485 nm, and emission spectra were collected in the range of 500–750 nm with slit widths of 5 nm for both excitation and emission (Fig. 6). A water blank containing an identical foam piece but without metal ions was also recorded for baseline correction.

Table 1 summarizes the analytical parameters, including slope, standard deviation (σ), limit of detection (LOD), R^2 value, and the type of fluorescence response. Distinct interaction was observed for each metal ion. As^{3+} exhibited a slope of 223.4, LOD of 0.0013 μM, and R^2 was 0.97. Cd^{2+} gave a similar enhancement (slope: 255.5, LOD: 0.011 μM, R^2: 0.835). Zn^{2+} induced a slightly stronger effect (slope: 307.8, LOD: 0.009 μM, R^2: 0.91) while Cu^{2+} elicited the highest response (slope: 601.9, LOD: 0.0049 μM, R^2: 0.92). Ca^{2+} also caused a significant enhancement (slope: 370.3, LOD: 0.0081 μM, R^2: 0.93). In contrast, the Ag^+ triggered fluorescence quenching characterized by a negative slope: −19.39, LOD: 0.15 μM, and R^2 of 0.945.
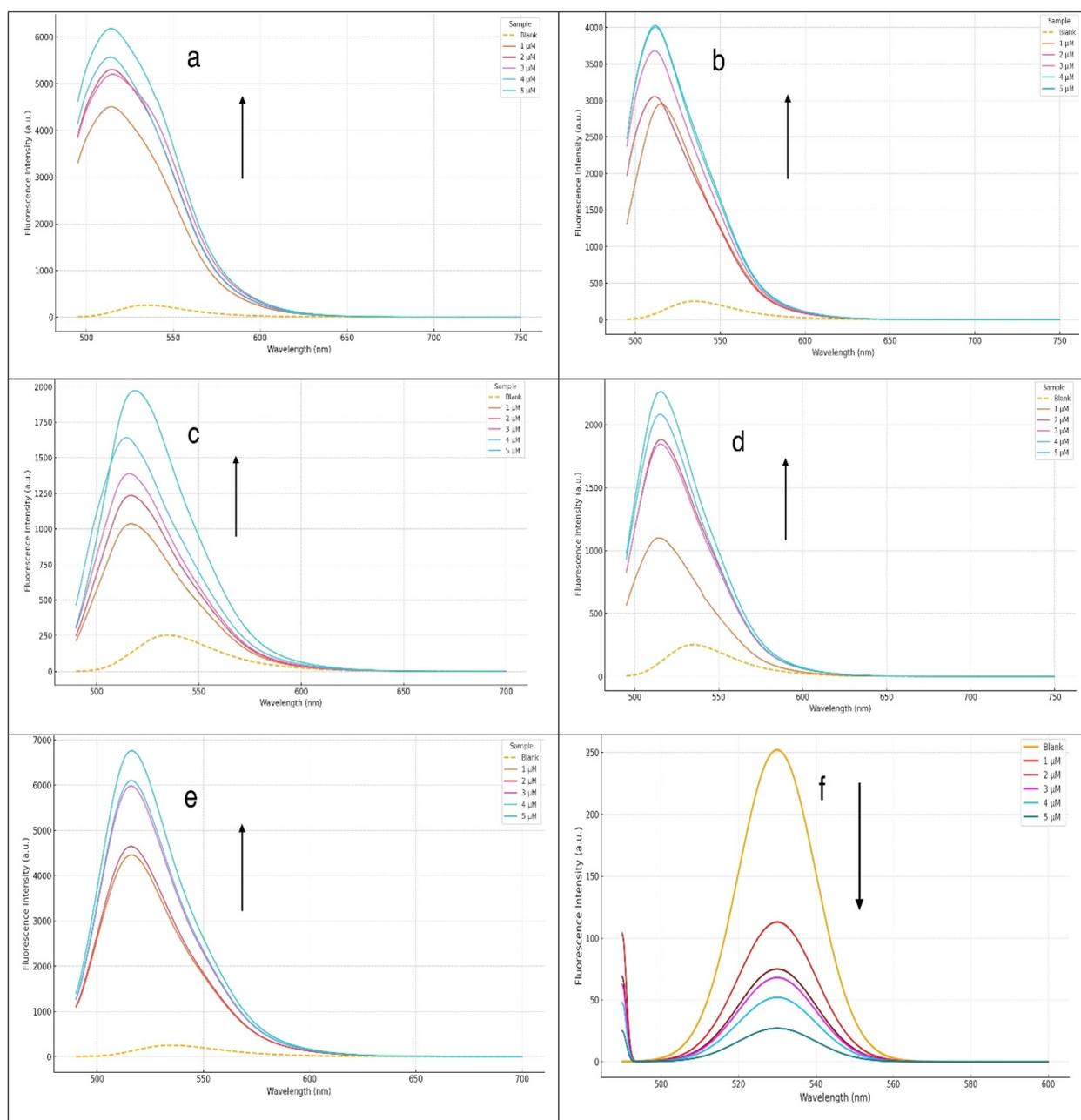

Fig. 6 Fluorescence emission spectra of PUF/UIO-66-NH-calcein in the presence of (a) Ca^{2+}, (b) Zn^{2+}, (c) As^{3+}, (d) Cd^{2+}, (e) Cu^{2+}, (f) Ag^+ (1–5 μM).

Table 1 Analytical parameters

Ion name	Slope	R^2	LOD	LOQ	LLR	Order	Equation
As^{3+}	223.4	0.9731	0.0013 μM	0.0039 μM	20 μM	3.7099	$Y = 223.4x + 792$
Cd^{2+}	255.5	0.8355	0.0049 μM	0.0147 μM	40 μM	3.4347	$Y = 255.5x + 1064.3$
Zn^{2+}	307.8	0.9105	0.009 μM	0.027 μM	50 μM	3.2676	$Y = 307.8x + 2619.6$
Cu^{2+}	601.9	0.9266	0.0049 μM	0.0098 μM	25 μM	3.4067	$Y = 601.9x + 3780.9$
Ca^{2+}	370.3	0.9350	0.0081 μM	0.0162 μM	35 μM	3.3345	$Y = 370.3x + 4238.5$
Ag^+	−19.39	0.945	0.15 μM	0.45 μM	10 μM	1.3467	$Y = -19.39x + 125.17$

For the silver acetate ion, significant quenching sensitivity was observed. Fluorescence spectra were recorded at concentrations of 1 to 4 μM of quencher, along with a blank. The emission peak was observed at 535 nm. The Stern–Volmer plot (F_0/F vs. [Quencher]) showed a moderately linear trend with R^2 of 0.972, indicating dynamic or static quenching behavior (Fig. 7). The Stern–Volmer quenching constant (K_{sv}) was calculated as 0.917 $μM^{-1}$, suggesting a high quenching efficiency of the silver acetate catalyst. The estimated slope ($b = 0.917$) indicates that for every one-unit increase in x, the predicted value of y increases by approximately 0.92 units on average. The 95% confidence interval for the slope ranges from 0.631 to 1.203, which does not include zero, suggesting that the linear relationship between x and y is statistically significant ($p = 0.002 < 0.05$). Similarly, the intercept ($a = 1.19$) has a 95% confidence interval of [0.49, 1.89], representing the expected value of y when $x = 0$. The regression model demonstrates a strong positive and statistically significant linear relationship between x and y. Given the small standard errors and narrow confidence intervals, the estimated parameters are reliable and precise. The model provides a good fit to the observed data (Table 2).

3.7. Mechanistic insights and sensitivity

The increased fluorescence intensities in response to As^{3+}, Cd^{2+}, Zn^{2+}, Cu^{2+}, and Ca^{2+} are likely attributed to the chelation-enhanced fluorescence (CHEF) effect. Among the tested ions,
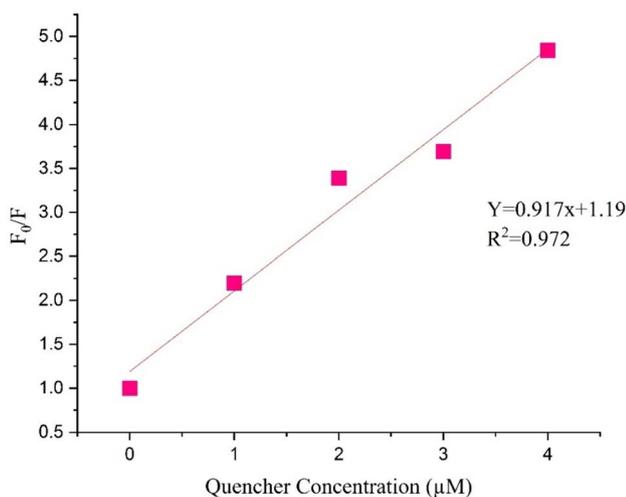

Fig. 7 The Stern–Volmer plot (F_0/F vs. [Quencher]) of silver acetate.

Table 2 Observed data used for the simple linear regression analysis

Parameter	Estimate	Standard error	95% confidence interval
Intercept (a)	1.19	0.22	[0.49, 1.89]
Slope (b)	0.917	0.0898	[0.631, 1.203]

Cu^{2+} showed the highest quantity, followed by Ca^{2+} and Zn^{2+}. In contrast, Ag^+ caused fluorescence quenching, possibly due to either dynamic or static quenching mechanisms. Overall, the lowest LOD values make the sensor suitable for detecting trace levels of metal ions in environmental and medical samples.

3.8. Repeatability and reuse

The PUF/UIO-66-NH–calcein nanocomposite was evaluated for its reusability and operational stability by performing four consecutive sensing experiments upon regeneration via simple washing with aqueous ethanol and fresh distilled water. Throughout these repeated cycles, the fluorescence intensity remained consistent, with negligible variation observed in the emission signal (Fig. 8). This sustained performance indicates that the sensor maintains its structural integrity and active sensing sites during multiple uses, highlighting its robustness. The demonstrated stability under repeated exposure conditions underscores the sensor's potential for practical applications where reusability and reliable performance over time are critical, reducing the need for frequent replacement and enhancing cost-effectiveness. For this purpose, the composite sensor was reused in consecutive sensing cycles; the material was regenerated between cycles to restore the available binding sites. After every fluorescence measurement, the foam sensor was sequentially washed first with ethanol to remove physically adsorbed species and then with distilled water to eliminate residual ions and neutralize the surface. As a result, the sensor recovers its original fluorescence behavior before each new cycle. Therefore, the nearly constant fluorescence intensity observed over repeated cycles is attributed to efficient mild regeneration of the sensing sites. This confirms that the fluorescence enhancement follows a reversible chelation-enhanced fluorescence (CHEF) mechanism and demonstrates the excellent reusability and operational stability of the PUF/UiO-66-NH₂–Calcein composite."

3.9. Selectivity evaluation

The fluorescence responses of PUF/UiO-66-NH–calcein toward various metal cations (5 μM) were investigated at different pH
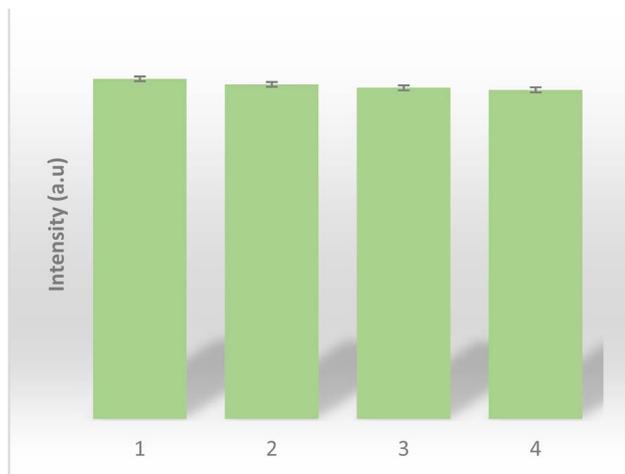
Fig. 8 Fluorescence intensity in the recyclability studies of the PUF/UIO-66-NH–calcein after four cycles of use in copper solution.

values to evaluate the selectivity. As shown in (Fig. 9a), the sensor exhibited a great fluorescence response for Cu^{2+} in the presence of other metal ions, including Zn^{2+}, Ag^+, Cd^{2+}, Ca^{2+}, and As^{3+} at neutral pH. Interestingly, the fluorescence intensities remarkably changed upon adjusting the pH to 5, and a distinct enhancement was observed mainly for Cu^{2+} and Zn^{2+}

ions. Among them, Cu^{2+} induced the most pronounced fluorescence intensity, while other cations caused negligible or no spectral variation under the same conditions.

Fluorescence intensity of PUF/UiO-66-NH–calcein upon addition of Cu^{2+} (5 μM) in the presence of various interfering metal cations was investigated at pH 5, as seen in (Fig. 9b). The obtained results suggest that PUF/UiO-66-NH–calcein nanocomposite demonstrates pH-dependent selectivity, acting as an efficient responsive Cu^{2+} fluorescent probe under mild acidic conditions (pH 5). As shown in Fig. 9d, at pH 7, the sensor exhibits a strong fluorescence response in the presence of multiple metal ions, including Cu^{2+}, Zn^{2+}, Ag^+, Cd^{2+}, Ca^{2+}, and As^{3+}. This result specifies that the sensing platform has no selectivity under neutral conditions, as several cations are able to interact efficiently with the calcein moieties and induce fluorescence enhancement.

In contrast, upon adjusting the medium to pH 5, a marked change in fluorescence behavior is observed (Fig. 9c). Under the mild acidic condition, a distinct and dominant fluorescence enhancement is induced by Cu^{2+}, while the responses of other competing metal ions become negligible. Importantly, when Cu^{2+} is introduced in the presence of all other coexisting cations, no noticeable suppression or interference is detected, confirming that Cu^{2+} maintains its fluorescence turn-on behavior even in complex ionic environments. At pH 5,
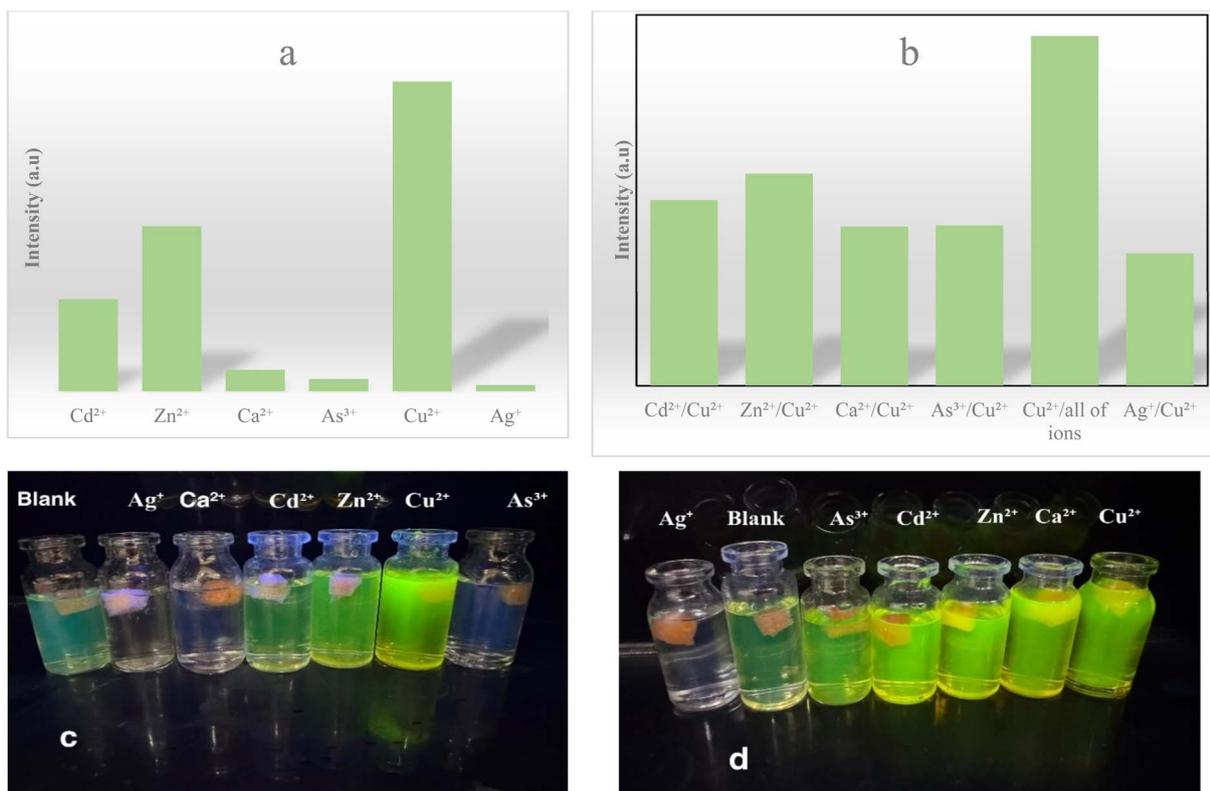

Fig. 9 Fluorescence intensity of (a) PUF/UIO-66-NH–calcein toward various metal (5 μM) in pH 5), (b) fluorescence intensity of PUF/UIO-66-NH–calcein toward various metal upon addition of Cu^{2+} in the presence of various metal cations in pH 5 aqueous solution, (c) effect of fluorescence intensity of PUF/UIO-66-NH–Calcein toward various metal in pH 5, (d) effect of fluorescence intensity of PUF/UIO-66-NH–Calcein toward various metal in pH 7.

Table 3 Comparative fluorescence response of individual components and composite toward Cu^{2+} at pH 5 and pH 7

Material	pH	Structural stability in water	Fluorescence response to cu^{2+}	Selectivity
PUF	5 and 7	Stable foam	—	—
Uio-66-NH$_2$	5 and 7	Stable suspension	—	—
PUF/Calcein	5 and 7	Calcein leaching	Strong	Non-selective
PUF/UIO-66-NH–calcein	5	Stable/no leaching	Strong	Selective
PUF/UIO-66-NH–calcein	7	Stable/no leaching	Strong	Limited

a systematic selectivity assessment was performed to clearly validate the preferential recognition of Cu^{2+}. Initially, the fluorescence response of the PUF/UiO-66-NH–calcein composite was recorded individually in the presence of each metal ion (5 μM) under identical experimental conditions. Among all tested cations, Cu^{2+} generated the most pronounced fluorescence enhancement. To further evaluate competitive effects, 5 μM of Cu^{2+} was subsequently combined separately with each of the metal ions, maintaining the same total concentration and pH conditions. In all cases, the fluorescence intensity remained comparable to that induced by Cu^{2+} alone, indicating that coexisting ions did not significantly interfere with the Cu^{2+}-triggered emission. These results confirm that the dominant fluorescence signal originates from the strong coordination interaction between Cu^{2+} and the calcein moieties, thereby demonstrating effective and reliable selective recognition of Cu^{2+} under mild acidic conditions (Fig. 9b).

The enhanced selectivity at this pH is likely due to partial protonation of the amino groups and modulation of coordination sites, favoring the strong binding affinity of Cu^{2+} ions compared to other cations. Furthermore, no significant interference with the Cu^{2+}-induced fluorescence enhancement was detected when all metal ions were added simultaneously. This clearly indicates that under mild acidic conditions (pH 5), the PUF/UiO-66-NH–calcein nanocomposite exhibits an almost selective recognition behavior toward Cu^{2+} ions. This observation confirms that the sensor exhibits strong selectivity toward Cu^{2+} with (slope: 263.3, LOD: 0.011 μM, R^2: 0.9247) at mildly acidic conditions (Fig. 9c), and the fluorescence turn-on response can be attributed to the tight coordination interaction between Cu^{2+} and the calcein moieties anchored on the UIO-66-NH$_2$ framework. Complexation of metal ions requires ligands containing heteroatoms with electron pairs. Generally, higher pH favors complex formation due to deprotonation of donor sites; however, for ions such as Ag^+, excessive alkalinity promotes the formation of insoluble hydroxides or hydroxo complexes, which prevent coordination and fluorescence response. Moreover, while higher pH values can enhance fluorescence intensity through increased conjugation between heteroatoms and the aromatic π-system, lower pH leads to protonation and nonradiative relaxation, resulting in fluorescence quenching. Considering both effects, a mildly acidic condition (pH 5) was chosen as the optimal environment for stable complex formation and selective fluorescence sensing of Cu^{2+}ions.

"Control experiments were performed to clarify the individual contributions of PU foam, UiO-66-NH$_2$, and PUF-calcein toward the overall sensing behavior. As shown in Table 3, neither pristine PU foam nor UiO-66-NH$_2$ exhibited any noticeable fluorescence response toward Cu^{2+} at either pH 5 or pH 7, confirming that these components are optically inactive and mainly serve as structural supports. As expected, PUF-calcein demonstrated fluorescence enhancement in aqueous solution; however, it suffers from non-recoverability, poor selectivity, and responds similarly to various metal ions at both pH values. In contrast, the PUF/UiO-66-NH–calcein composite showed significantly improved fluorescence intensity, excellent stability in water, and pronounced Cu^{2+} selectivity at pH 5. These results demonstrate a clear synergistic effect between calcein, UiO-66-NH$_2$, and the PU matrix, where the MOF provides immobilization sites for calcein, and the PU matrix offers mechanical stability and accessibility, collectively leading to enhanced sensitivity, selectivity, and durability of the composite sensor."

3.10. Real sample analysis

To evaluate the practical applicability of the fabricated PUF/UiO-66-NH$_2$–calcein sensor, fluorescence measurements were carried out using real local water samples. Seawater was
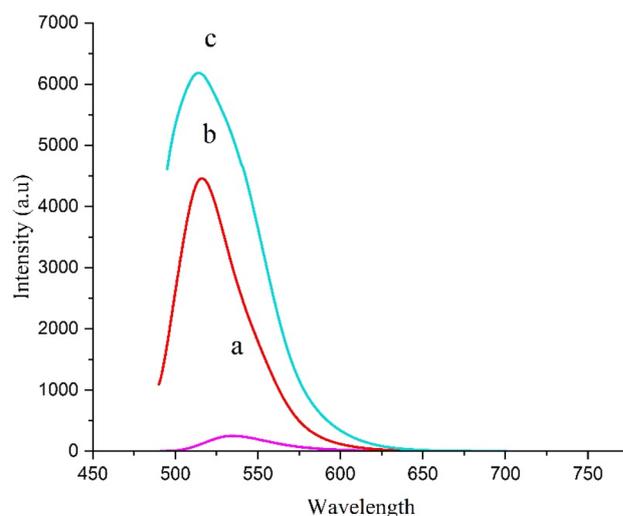

Fig. 10 Fluorescence emission spectra of PUF/UIO–66–NH–calcein in the presence of (a) blank (b) Tejen river in pH 5 (c) Caspian Sea in pH 5.

Table 4 Comparison of fluorescent sensors for copper ion detection

Material/System	Target ions	LOD (μM)	Response type	Reference
MOF [PCN-224]	Cu^{2+}	0.000068	Quenching	31
4-(2-aminomethyl)pyridine-*N*-allylnaphthalimide	Cu^{2+}	0.11	Quenching	32
Eu-MOF	Cu^{2+}, Ni^{2+}	4.69, 1.47	Turn-off	33
oxOPD	Cu^{2+}, pyrophosphate ion	0.023, 0.0007	Quenching	34
EuTb-MOFs	Cu^{2+}, Pb^{2+}	0.037, 0.041	Quenching	35
Porphyrin MOF	Cu^{2+}	0.000068	Quenching	36
(CdTe) quantum dots (QDs)	Cu^{2+}	20	Ratiometric	37
Zn-MOF	Hg^{2+}, CrO_4^{2-} and $Cr_2O_7^{2-}$	0.01	Colorimetric	38
Pyridine based receptor	Cu^{2+}	0.25	Colorimetric	39
PUF/UiO-66-NH–calcein	**Cu^{2+}, Zn^{2+}, As^{3+}etc.**	**0.0049, 0.009, 0.013**	**Enhancement/Quenching**	**This work**

collected from the Caspian Sea (Babolsar, Iran), and river water was obtained from the Tajan River (Sari, Iran). Prior to analysis, the samples were filtered to remove suspended particulates and directly subjected to fluorescence sensing without any additional pretreatment.

Upon immersion of the sensor foam into the real samples under the optimized conditions (pH 5), a distinct fluorescence response was observed. The Caspian Sea water sample exhibited a fluorescence intensity of approximately 0.4 ppm while the Tejen River water sample showed a lower intensity of about 0.19 ppm, indicating different Cu^{2+} levels in the two water sources (Fig. 10). To verify the accuracy of the fluorescence-based results, the same samples were analyzed by atomic absorption spectroscopy (AAS) as a reference method. The AAS measurements revealed a copper concentration of approximately 0.4 ppm in the seawater sample and about 0.2 ppm in the river water sample. The higher fluorescence intensity obtained for the seawater sample is therefore consistent with its higher Cu^{2+} concentration determined by AAS. These results demonstrate a good agreement between the fluorescence sensor response and the standard analytical technique, confirming the reliability and practical feasibility of the proposed sensor for real-time monitoring of Cu^{2+} ions in environmental water samples.

3.11. Extended novelty statement

The fluorescent sensing platform developed in this work exhibits several distinct advantages compared with recently reported MOF-based metal-ion sensors (Table 4). Unlike many literature examples in which selective Cu^{2+} detection is mainly performed based on fluorescence quenching mechanisms,[31–36] the present composite showed a pronounced fluorescence enhancement toward Cu^{2+}. It is highly desirable for achieving clearer signal readout and improved signal-to-noise ratios. The sensing system is constructed through covalent immobilization of calcein onto UiO-66-NH₂, followed by integration within a flexible polyurethane (PU) foam matrix. This rational design endows the composite with multiple synergistic benefits, including efficient retention of the fluorophore, suppression of dye leaching, enhanced mechanical robustness, and facile handling in reusable solid-state formats. In contrast to many previously reported sensors that require buffered media,

organic co-solvents, or sophisticated excitation sources, the proposed sensor operates efficiently in distilled water at ambient temperature without additional chemical modification or complex instrumentation.

Furthermore, the composite displays dual-mode fluorescence behavior, exhibiting enhancement toward Cu^{2+}, Zn^{2+}, Ca^{2+}, Cd^{2+}, and As^{3+} at pH 7, and showing quenching in the presence of Ag^+. This dual response enables discrimination among different classes of metal ions and broadens the analytical versatility of the platform. The achieved low micromolar and sub-micromolar detection limits are comparable to or superior to many previously reported MOF-based sensors, despite the markedly simpler fabrication route.

Notably, the PUF/UiO-66-NH₂–calcein composite maintains stable fluorescence performance over at least five successive sensing cycles without requiring harsh chemical treatment for regeneration, highlighting its excellent operational simplicity and stability. The combination of fluorescence enhancement-based detection, mechanical flexibility, reusability, and straightforward synthesis renders this sensing platform a practical and competitive alternative to existing MOF-based optical sensors for real-world environmental monitoring.

4. Conclusion

In summary, a robust and water-compatible fluorescent sensing platform based on UiO-66-NH₂–calcein immobilized within a polyurethane foam matrix was successfully developed for metal-ion detection in aqueous environments. Comprehensive structural and morphological characterizations (XRD, FT-IR, TGA, BET, and FE-SEM) verified that the crystalline framework of UiO-66-NH₂ remains intact after calcein functionalization and subsequent incorporation into the PU matrix. The three-dimensional porous structure of the foam provides efficient diffusion pathways, improved mass transfer, and excellent mechanical stability.

Fluorescence studies demonstrated that the composite exhibits a pronounced and selective fluorescence enhancement toward Cu^{2+} under mildly acidic conditions (pH 5), while other investigated metal ions, including Zn^{2+}, Ag^+, Cd^{2+}, Ca^{2+}, and As^{3+}, induce considerably weaker responses. Moreover, competition experiments confirmed that the Cu^{2+}-induced fluorescence signal is well preserved in the presence of

coexisting ions, highlighting the practical selectivity without the interference of other cations.

This work illustrates that embedding MOF–fluorophore hybrid into a flexible polymer scaffold is an effective strategy to enhance optical activity while simultaneously improving stability, accessibility, and reusability. Owing to its simple fabrication, fast response, operation in water, and good mechanical durability, the PU/UiO-66-NH$_2$–calcein composite represents a promising candidate for low-cost, portable, and field-deployable fluorescence sensing of Cu^{2+} in environmental aqueous samples.

Conflicts of interest

The authors declare that there is no conflict of interest regarding the publication of this manuscript.

Data availability

All data generated or analyzed during this study are included in this published article.

Supplementary information (SI): TGA and BET graphs. See DOI: https://doi.org/10.1039/d5ra09900e.

Acknowledgements

References

1 E. David and C. Cosio, New Insights into Impacts of toxic metals in aquatic environments, *Environments*, 2020, **8**(1), 1, DOI: 10.3390/environments8010001.

2 Y. Ding, C. Deng, Y. Yang, J. Zhang, W. Liu, O. Aras, F. An, J. Liu and Y. Chai, Carrier-free nanoparticles for cancer theranostics with dual-mode magnetic resonance imaging/fluorescence imaging and combination photothermal and chemodynamic therapy, *Int. J. Pharm.*, 2025, **671**, 125285, DOI: 10.1016/j.ijpharm.2025.125285.

3 M. Ali, N. Memon, M. A. Mallah, A. S. Channa, R. Gaur and Y. Jiahai, Recent development in fluorescent probes for copper ion detection, *Curr. Top. Med. Chem.*, 2022, **22**(10), 835–854, DOI: 10.2174/1568026622666220225153703.

4 Z. Gerdan, Y. Saylan and A. Denizli, Recent advances of optical sensors for copper ion detection, *Micromachines*, 2022, **13**(8), 1298, DOI: 10.3390/mi13081298.

5 C. Guo, L. Lv, Y. Liu, M. Ji, E. Zang, Q. Liu, M. Zhang and M. Li, Applied analytical methods for detecting heavy metals in medicinal plants, *Crit. Rev. Anal. Chem.*, 2023, **53**(2), 339–359, DOI: 10.1080/10408347.2021.1953371.

6 L. A. Malik, A. Bashir, A. Qureashi and A. H. Pandith, Detection and removal of heavy metal ions: a review, *Environ. Chem. Lett.*, 2019, **17**(4), 1495–1521, DOI: 10.1007/s10311-019-00891-z.

7 M. Li, Q. Shi, N. Song, Y. Xiao, L. Wang, Z. Chen and T. D. James, Current trends in the detection and removal of heavy metal ions using functional materials, *Chem. Soc. Rev.*, 2023, **52**(17), 5827–5860, DOI: 10.1039/D2CS00683A.

8 J. A. Buledi, S. Amin, S. I. Haider, M. I. Bhanger and A. R. Solangi, A review on detection of heavy metals from aqueous media using nanomaterial-based sensors, *Environ. Sci. Pollut. Res.*, 2021, **28**(42), 58994–59002, DOI: 10.1007/s11356-020-07865-7.

9 Z. Hu, W. Long, T. Liu, Y. Guan, G. Lei, Y. Suo, M. Jia, J. He, H. Chen, Y. She and H. Fu, A sensitive fluorescence sensor based on a glutathione modified quantum dot for visual detection of copper ions in real samples, *Spectrochim. Acta A Mol. Biomol. Spectrosc.*, 2023, **294**, 122517, DOI: 10.1016/j.saa.2023.122517.

10 T. Mayr and T. Werner, Highly selective optical sensing of copper (II) ions based on fluorescence quenching of immobilised Lucifer Yellow, *Analyst*, 2002, **127**(2), 248–252, DOI: 10.1039/B106298K.

11 J. Kumar, P. K. Bhattacharyya and D. K. Das, New duel fluorescent "on–off" and colorimetric sensor for Copper (II): Copper (II) binds through N coordination and pi cation interaction to sensor, *Spectrochim. Acta A Mol. Biomol. Spectrosc.*, 2015, **138**, 99–104, DOI: 10.1016/j.saa.2014.11.030.

12 Y. Xue, Y. Peng, Z. Geng, Y. Wang, C. O. Ung and H. Hu, Metal—Organic Frameworks (MOFs) Based Analytical Techniques for Food Safety Evaluation, *eFood*, 2021, **2**(1), 1–2, DOI: 10.2991/efood.k.210209.00.

13 P. V. Mane, R. M. Rego, P. L. Yap, D. Losic and M. D. Kurkuri, Unveiling cutting-edge advances in high surface area porous materials for the efficient removal of toxic metal ions from water, *Prog. Mater. Sci.*, 2024, **146**, 101314, DOI: 10.1016/j.pmatsci.2024.101314.

14 D. Zhao, S. Yu, W. J. Jiang, Z. H. Cai, D. L. Li, Y. L. Liu and Z. Z. Chen, Recent progress in metal-organic framework based fluorescent sensors for hazardous materials detection, *Molecules*, 2022, **27**(7), 2226, DOI: 10.3390/molecules27072226.

15 T. Wu, X. J. Gao, F. Ge and H. G. Zheng, Metal–organic frameworks (MOFs) as fluorescence sensors: principles, development and prospects, *CrystEngComm*, 2022, **24**(45), 7881–7901, DOI: 10.1039/D2CE01159J.

16 M. H. Yu, T. L. Hu and X. H. Bu, A metal–organic framework as a "turn on" fluorescent sensor for aluminum ions, *Inorg. Chem. Front.*, 2017, **4**(2), 256–260, DOI: 10.1039/C6QI00362A.

17 C. Jia, T. He and G. M. Wang, Zirconium-based metal-organic frameworks for fluorescent sensing, *Coord. Chem. Rev.*, 2023, **476**, 214930, DOI: 10.1016/j.ccr.2022.214930.

18 Y. Bai, Y. Dou, L. H. Xie, W. Rutledge, J. R. Li and H. C. Zhou, Zr-based metal–organic frameworks: design, synthesis, structure, and applications, *Chem. Soc. Rev.*, 2016, **45**(8), 2327–2367, DOI: 10.1039/C5CS00837A.

19 Q. Du, R. Rao, F. Bi, Y. Yang, W. Zhang, Y. Yang, N. Liu and X. Zhang, Preparation of modified zirconium-based metal-organic frameworks (Zr-MOFs) supported metals and recent application in environment: a review and

perspectives, *Surf. Interfaces*, 2022, **28**, 101647, DOI: 10.1016/j.surfin.2021.101647.

20 X. Y. Xu and B. Yan, Eu (III) functionalized Zr-based metal-organic framework as excellent fluorescent probe for Cd^{2+} detection in aqueous environment, *Sensor. Actuator. B Chem.*, 2016, **222**, 347–353, DOI: 10.1016/j.snb.2015.08.082.

21 W. Lv, Y. Song, R. Guo, N. Liu and Z. Mo, Zirconium-based metal–organic framework encapsulated dye molecules: An excellent sensing platform for sensitive detection of Cu^{2+} in aqueous environments, *Spectrochim. Acta A Mol. Biomol. Spectrosc.*, 2024, **310**, 123883, DOI: 10.1016/j.saa.2024.123883.

22 D. Bratosin, L. Mitrofan, C. Palii, J. Estaquier and J. Montreuil, Novel fluorescence assay using calcein-AM for the determination of human erythrocyte viability and aging, *Cytom. J. Int. Soc. Anal. Cytol.*, 2005, **66**(1), 78–84, DOI: 10.1002/cyto.a.20152.

23 M. K. Tufail, M. Ifrahim, M. Rashid, I. U. Haq, R. Asghar, U. T. Uthappa, M. Selvaraj and M. Kurkuri, Chemistry of zeolites and zeolite based composite membranes as a cutting-edge candidate for removal of organic dyes & heavy metal ions: Progress and future directions, *Sep. Purif. Technol.*, 2025, **354**, 128739, DOI: 10.1016/j.seppur.2024.128739.

24 J. Li, Y. Hou, H. Wu, C. Chen, X. Fu, J. Liu, L. Li, S. Shang and G. Deng, A poly (vinyl alcohol) coated core-shell nanoparticle with a tunable surface for pH and glutathione dual-responsive drug delivery, *Colloids Surf. B Biointerfaces*, 2025, **247**, 114421, DOI: 10.1016/j.colsurfb.2024.114421.

25 M. Ates, S. Karadag, A. A. Eker and B. Eker, Polyurethane foam materials and their industrial applications, *Polym. Int.*, 2022, **71**(10), 1157–1163, DOI: 10.1002/pi.6441.

26 N. V. Gama, A. Ferreira and A. Barros-Timmons, Polyurethane foams: Past, present, and future, *Materials*, 2018, **11**(10), 1841, DOI: 10.3390/ma11101841.

27 Y. Cao, H. Zhang, F. Song, T. Huang, J. Ji, Q. Zhong, W. Chu and Q. Xu, UiO-66-NH$_2$/GO composite: synthesis, characterization and CO^2 adsorption performance, *Materials*, 2018, **11**(4), 589, DOI: 10.3390/ma11040589.

28 I. Amundarain, R. Miguel-Fernández, A. Asueta, S. García-Fernández and S. Arnaiz, Synthesis of rigid polyurethane foams incorporating polyols from chemical recycling of post-industrial waste polyurethane foams, *Polymers*, 2022, **14**(6), 1157, DOI: 10.3390/polym14061157.

29 N. Jadhav, S. N. Kumar, P. S. Tanvidkar and B. V. Kuncharam, Synthesis and characterization of mixed-matrix material of Zirconium based metal organic framework (MOF: UiO-66-NH$_2$) and poly (ether-urethane-urea), *Mater. Today: Proc.*, 2020, **28**, 734–738, DOI: 10.1016/j.matpr.2019.12.289.

30 W. Li and S. Liu, Preparation and characterization of polyurethane foam/activated carbon composite adsorbents, *J. Porous Mater.*, 2012, **19**(5), 567–572, DOI: 10.1007/s10934-011-9506-5.

31 J. Chen, H. Chen, T. Wang, J. Li, J. Wang and X. Lu, Copper ion fluorescent probe based on Zr-MOFs composite material, *Anal. Chem.*, 2019, **91**(7), 4331–4336, DOI: 10.1021/acs.analchem.8b03924.

32 Z. Xu, P. Deng, J. Li and S. Tang, Fluorescent ion-imprinted sensor for selective and sensitive detection of copper (II) ions, *Sensor. Actuator. B Chem.*, 2018, **255**, 2095–2104, DOI: 10.1016/j.snb.2017.09.007.

33 B. Kabak and E. Kendüzler, Europium metal-organic frameworks: Synthesis, characterization, and application as fluorescence sensors for the detection of Cu^{2+}, Ni^{2+} cations and T3, T4 hormones, *Talanta*, 2024, **266**, 124944, DOI: 10.1016/j.talanta.2023.124944.

34 W. J. Zhang, S. G. Liu, L. Han, H. Q. Luo and N. B. Li, A ratiometric fluorescent and colorimetric dual-signal sensing platform based on N-doped carbon dots for selective and sensitive detection of copper (II) and pyrophosphate ion, *Sensor. Actuator. B Chem.*, 2019, **283**, 215–221, DOI: 10.1016/j.snb.2018.12.012.

35 Y. Gao, Y. Zhu, Y. Wang and J. Bi, Water-Stable Ln-MOF as a multi-emitting luminescent sensor for the detection of metal ions and pharmaceuticals, *Spectrochim. Acta A Mol. Biomol. Spectrosc.*, 2024, **323**, 124915, DOI: 10.1016/j.saa.2024.124915.

36 W. Zhou, Z. Hu, J. Wei, H. Lu, H. Dai, J. Zhao, W. Zhang and R. Guo, A ratiometric fluorescent probe based on PCN-224 for rapid and ultrasensitive detection of copper ions, *Compos. Commun.*, 2022, **33**, 101221, DOI: 10.1016/j.coco.2022.101221.

37 Y. Wang, C. Zhang, X. Chen, B. Yang, L. Yang, C. Jiang and Z. Zhang, Ratiometric fluorescent paper sensor utilizing hybrid carbon dots–quantum dots for the visual determination of copper ions, *Nanoscale*, 2016, **8**(11), 5977–5984, DOI: 10.1039/C6NR00430J.

38 J. Xiao, J. Liu, X. Gao, G. Ji, D. Wang and Z. Liu, A multi-chemosensor based on Zn-MOF: Ratio-dependent color transition detection of Hg (II) and highly sensitive sensor of Cr (VI), *Sensor. Actuator. B Chem.*, 2018, **269**, 164–172, DOI: 10.1016/j.snb.2018.04.129.

39 D. Mohanasundaram, R. Bhaskar, M. Sankarganesh, K. Nehru, G. G. Kumar and J. Rajesh, A simple pyridine based fluorescent chemosensor for selective detection of copper ion, *Spectrochim. Acta A Mol. Biomol. Spectrosc.*, 2022, **265**, 120395, DOI: 10.1016/j.saa.2021.120395.